

A 64mW DNN-based Visual Navigation Engine for Autonomous Nano-Drones

Daniele Palossi, Antonio Loquercio, Francesco Conti, Eric Flamand, Davide Scaramuzza, Luca Benini

Abstract—Fully-autonomous miniaturized robots (e.g., drones), with artificial intelligence (AI) based visual navigation capabilities are extremely challenging drivers of Internet-of-Things edge intelligence capabilities. Visual navigation based on AI approaches, such as deep neural networks (DNNs) are becoming pervasive for standard-size drones, but are considered out of reach for nano-drones with size of a few cm². In this work, we present the first (to the best of our knowledge) demonstration of a navigation engine for autonomous nano-drones capable of closed-loop end-to-end DNN-based visual navigation. To achieve this goal we developed a complete methodology for parallel execution of complex DNNs directly on-board of resource-constrained milliwatt-scale nodes. Our system is based on GAP8, a novel parallel ultra-low-power computing platform, and a 27 g commercial, open-source CrazyFlie 2.0 nano-quadrotor. As part of our general methodology we discuss the software mapping techniques that enable the state-of-the-art deep convolutional neural network presented in [1] to be fully executed on-board within a strict 6fps real-time constraint with no compromise in terms of flight results, while all processing is done with only 64 mW on average. Our navigation engine is flexible and can be used to span a wide performance range: at its peak performance corner it achieves 18 fps while still consuming on average just 3.5% of the power envelope of the deployed nano-aircraft.

Index Terms—Unmanned Autonomous Vehicles, Convolutional Neural Networks, Ultra-low-power

I. INTRODUCTION

With the rise of the Internet-of-Things (IoT) era and rapid development of artificial intelligence (AI), embedded systems ad-hoc programmed to act in relative isolation are being progressively replaced by AI-based sensor nodes that acquire information, process and understand it, and use it to interact with the environment and with each other. The “ultimate” IoT node will be that which will be capable of autonomously navigating the environment and, at the same time, sensing, analyzing, and understanding it [2].

This work has been partially funded by projects EC H2020 HERCULES (688860), by the Swiss National Science Foundation under grant 162524 (MicroLearn: Micropower Deep Learning), by the Swiss National Center of Competence Research (NCCR) Robotics and by the SNSF-ERC starting grant.

D. Palossi, F. Conti, E. Flamand and L. Benini are with the Integrated System Laboratory of ETH Zürich, ETZ, Gloriastrasse 35, 8092 Zürich, Switzerland (e-mail: dpalossi@iis.ee.ethz.ch, fconti@iis.ee.ethz.ch, eflamand@iis.ee.ethz.ch, lbenini@iis.ee.ethz.ch).

A. Loquercio and D. Scaramuzza are with the Robotic and Perception Group, at both the Dep. of Informatics (University of Zürich) and the Dep. of Neuroinformatics (University of Zürich and ETH Zürich), Andreasstrasse 15, 8050 Zurich, Switzerland.

F. Conti and L. Benini are also with the Department of Electrical, Electronic and Information Engineering of University of Bologna, Viale del Risorgimento 2, 40136 Bologna, Italy (e-mail: f.conti@unibo.it, luca.benini@unibo.it).

E. Flamand is also with GreenWaves Technologies, Pépinière Bergès, avenue des Papeteries, 38190 Villard-Bonnot, France (e-mail: eric.flamand@greenwaves-technologies.com).

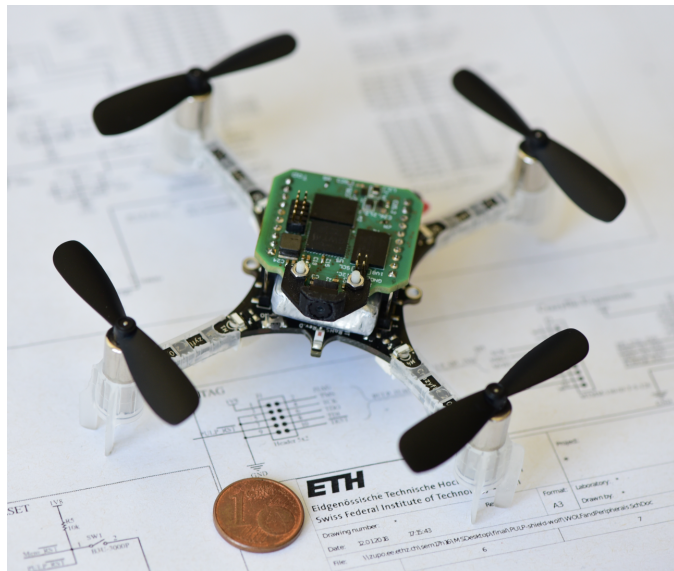


Fig. 1: Our prototype based on the COTS Crazyflie 2.0 nano-quadrotor extended with our *PULP-Shield*. The system is able to run the *DroNet* [1] CNN for autonomous visual navigation up to 18 fps using only on-board resources.

Fully autonomous nano-scale unmanned aerial vehicles (UAVs) are a befitting embodiments for this class of smart sensors: with their speed and agility, they have the potential to quickly collect information from both their on-board sensors and from a plethora of devices deployed in the environment. Nano-UAVs could also perform advanced on-board analytics, to pre-select essential information before transmitting it to centralized servers [3]. The tiny form-factor of nano-drones is ideal both for indoor applications where they should safely operate near humans (for surveillance, monitoring, ambient awareness, interaction with smart environments, etc.) [4] and for highly-populated urban areas, where they can exploit complementary sense-act capabilities to interact with the surroundings (e.g., smart-building, smart-cities, etc.) [5].

Commercial off-the-shelf (COTS) quadrotors have already started to enter the nano-scale, featuring only few centimeters in diameter and few tens of grams in weight [6]. However, commercial nano-UAVs still lack the autonomy boasted by their larger counterparts [1], [7], [8], [9], since their computational capabilities, heavily constrained by their tiny power envelopes, have been considered so far to be totally inadequate for the execution of sophisticated AI workloads, as summarized in Table I.

The traditional approach to autonomous navigation of an

TABLE I: Rotorcraft UAVs taxonomy by vehicle class-size.

Vehicle Class	\odot : Weight [cm:kg]	Power [W]	On-board Device
<i>std-size</i> [10]	$\sim 50 : \geq 1$	≥ 100	Desktop
<i>micro-size</i> [11]	$\sim 25 : \sim 0.5$	~ 50	Embedded
<i>nano-size</i> [12]	$\sim 10 : \sim 0.01$	~ 5	MCU
<i>pico-size</i> [13]	$\sim 2 : \leq 0.001$	~ 0.1	ULP

UAV is the so-called *localization-mapping-planning* cycle, which consists of estimating the robot motion using either offboard (e.g. GPS [14]) or onboard sensors (e.g., visual-inertial sensors [15]), building a local 3D map of the environment, and planning a safe trajectory through it [9]. These methods, however, are very expensive for computationally-constrained platforms. Recent results have shown that much lighter algorithms, based on convolutional neural networks (CNNs), are sufficient for enabling basic reactive navigation of small drones, even without a map of the environment [1], [16], [17], [18], [19]. However, their computational and power needs are unfortunately still above the allotted budget of current navigation engines of *nano* drones, which are based on simple, low-power microcontroller units (MCUs).

In Wood et al. [13], the authors indicate that, for small-size UAVs, the maximum power budget that can be spent for on-board computation is 5% of the total, the rest being used by the propellers (86%) and the low-level control parts (9%). The problem of bringing state-of-the-art navigation capabilities on the challenging classes of nano- and pico-size UAVs is therefore strictly dependent on the development of energy-efficient and computationally capable hardware, highly optimized software and new classes of algorithms combined together into a next-generation navigation engine. These constraints and requirements depict the same scenario faced in deploying high level computation capabilities on IoT edge-nodes/sensors. Moreover, in the case of a flying miniature robot, the challenge is exacerbated by the strict real-time constraint dictated by the need of fast reaction time in order to prevent collisions with dynamic obstacles.

Whereas standard-size UAVs with a power envelope of several hundreds Watts have always been able to host powerful high-end embedded computers like Qualcomm Snapdragon¹, Odroid, NVIDIA Jetson TX1 and TX2, etc., most nano-sized UAVs have been constrained by the capabilities of microcontroller devices capable to provide a few hundreds Mop/s at best. Therefore, CNN-based autonomous vision navigation was so far considered to be out of reach for this class of drones.

In this work, we propose a novel visual navigation engine and a general methodology to deploy complex CNN on top of COTS resources-constrained computational edge-nodes such as a nano-size flying robot. We present what, to the best of our knowledge, is the first deployment of a State-of-the-Art (SoA), fully autonomous vision-based navigation system based on deep learning on top of a UAV visual navigation engine consuming less than 284 mW at peak (64 mW in the most energy-efficient configuration), fully integrated and in closed-loop control within an open source COTS *CrazyFlie*

2.0 nano-UAV. Our visual navigation engine, shown on the top of the *CrazyFlie 2.0* in Figure 1, leverages the *Green-Waves Technologies GAP8* SoC, a high-efficiency embedded processor taking advantage of the emerging parallel ultra-low-power (PULP) computing paradigm to enable the execution of complex algorithmic flows onto power-constrained devices, such as nano-scale UAVs.

This work provides several contributions beyond the SoA of nano-scale UAVs and serves as a proof-of-concept for a larger class of AI-based applications in the IoT field. In this work:

- we developed a general methodology for deploying SoA deep learning algorithms on top of ultra-low power embedded computation nodes, as well as miniaturized robot;
- we adapted *DroNet*, the CNN-based approach for autonomous navigation proposed in Loquercio et al. [1] for standard-sized UAVs, to the computational requirements of a nano-sized UAV, such as fixed-point computation;
- we deployed *DroNet* on the *PULP-shield*, an ultra-low power visual navigation module featuring the GAP8 SoC, an ultra-low power camera and off-chip Flash/DRAM memory; the shield is designed as a pluggable PCB for the 27 g COTS *CrazyFlie 2.0* nano-UAV;
- we demonstrate our methodology for the *DroNet* CNN, achieving comparable quality of results in terms of UAV control with respect to the standard-sized baseline of [1] within an overall *PULP-shield* power budget of just 64 mW, achieving a throughput of 6 fps and up to 18 fps within 284 mW;
- we field-prove our methodology presenting a closed-loop fully functional demonstration of vision-driven autonomous navigation relying only on on-board resources.

Our work demonstrates that parallel ultra-low power computing is a viable solution to deploy autonomous navigation capabilities on-board nano-UAVs used as smart, mobile IoT endnodes, while at the same time showcasing a complete hardware/software methodology to implement such complex workloads on heavily power- and memory-constrained device.

The rest of the paper is organized as follows: Section II provides the SoA overview both in term of nano-UAVs and low-power IoT. In Section III introduces the software/hardware background of our work. Section IV presents in detail our CNN mapping methodology, including software tools and optimizations. Section V discusses the design of the visual navigation engine. Section VI-B shows the experimental evaluation of the work, considering both performance and power consumption, comparing our results with the SoA and also evaluating the final control accuracy. Finally, Section VII concludes the paper.

II. RELATED WORK

The development of the IoT is fueling a trend toward edge computing, to improve scalability, robustness, security [2]. While today's IoT edge nodes are usually stationary, autonomous nano-UAVs can be seen as perfect examples of next-generation IoT end-nodes, with high mobility and requiring an unprecedented level of on-board intelligence. The goal of this work is to make SoA visual autonomous navigation compatible with ultra-low power nano-drones, unlocking their deployment

¹ <https://developer.qualcomm.com/hardware/qualcomm-flight>

for IoT applications. Therefore, this section focuses on related work on nano-aircrafts [13] and the deployment of DNN on top of low-power IoT nodes.

The traditional approach to autonomous navigation of *nano*-drones requires to offload the computation to some remote, powerful base-station. For instance, the authors of [20] developed a visual-inertial simultaneous localization and mapping (SLAM) algorithm, for a 25 g nano quadrotor. The SLAM algorithm was used to stabilize the robot and follow a reference trajectory. All the computation was performed off-board, by streaming video and inertial information from the drone to a remote, power-unconstrained laptop. The main problems with this class of solutions are latency, maximum communication distance, reliability issues due to channel noise, and high on-board power-consumption due to the high-frequency video streaming.

Nano-size flying robots showing some autonomous navigation capability based only on their on-board computational resources have also been presented. In [12] the authors developed a 4 g stereo-camera and proposed a velocity estimation algorithm able to run on the MCU on-board a 40 g flying robot. If on one side this solution allows the drone to avoid obstacles during the flight, it still requires favorable flight conditions (e.g., low flight speed of 0.3 m/s). In [21] an optical-flow-based guidance system was developed for a 46 g nano-size UAV. The proposed ego-motion estimation algorithm did not rely on feature tracking, making it possible to run on the on-board MCU. Unfortunately, the autonomous functionality was limited to hovering and the method did not reach the accuracy of computationally expensive techniques based on feature tracking.

In [22], an application-specific integrated circuit (ASIC), called *NAVION*, for on-board visual-inertial odometry was presented. Although this chip exposes enough computational power to perform state estimation up to 171 fps within 24 mW, this represents only one among other basic functionalities required by any UAV to be fully autonomous. Therefore, in a real use case the proposed ASIC would still need to be paired with additional circuits, both for complementary on-board computation as well as for interacting with the drone’s sensors. Moreover, to the date, the *NAVION* accelerator does not reach the same level of maturity and completeness of our work; in fact, *NAVION* has not yet been demonstrated on a real-life flying nano-drone.

COTS nano-size quadrotors, like the *Bitcraze Crazyflie 2.0* or the *Walkera QR LadyBug*, typically embed on-board low-power single core MCUs, like the *ST Microelectronics STM32F4* [12], [20], [23]. While significant work has been done within academia [24], [25], [26] and industry (e.g. TensorFlow Lite² and ARM Compute Library³) to ease the embedding of deep neural networks on mobile ARM-based SoC’s, there is no common consensus yet on how to “correctly” deploy complex AI-powered algorithms, such a deep neural networks, on this class of low-power microcontrollers. This is a “hard” problem both in terms of resource management (in particular available working memory and storage) and the peak throughput achievable by single core MCUs. This

problem is furthermore exacerbated by a lack of abstraction layers and computing facilities that are taken for granted by customary deep learning tools, such as linear algebra libraries (e.g. BLAS, CUBLAS, CUDNN) and preprocessing libraries (e.g. OpenCV).

ARM has recently released CMSIS-NN [27], which is meant to shrink this gap by accelerating deep inference compute kernels on Cortex-M microcontroller platforms, providing the equivalent of a BLAS/CUDNN library (in Section VI-B we present a detailed SoA comparison between our results and CMSIS-NN). However, this effort does not curtail the difficulty of effectively deploying DNNs in memory-scarce platforms, which often requires special scheduling/tiling [28], [29] and is still widely considered an open problem.

Pushing beyond the aforementioned approaches, in this work we propose and demonstrate a visual navigation engine capable of sophisticated workloads, such as real-time CNN-based autonomous visual navigation [1], entirely on-board within the limited power envelope of nano-scale UAVs (~ 0.2 W)—whereas approaches of this complexity have been previously limited to standard-sized UAVs with external server-based computation or power hungry processors (≥ 10 W).

III. BACKGROUND

In this section we summarize the hardware/software background underlying our visual navigation engine. We first present the original *DroNet* CNN developed for standard-size UAVs. Then, we introduce the GAP8 SoC used on-board of our nano-drone.

A. *DroNet*

DroNet is a lightweight residual CNN architecture. By predicting the steering angle and the collision probability, it enables safe autonomous flight of a quadrotor in various indoor and outdoor environments.

The *DroNet* topology, as illustrated in Figure 2, was inspired by residual networks [30] and was reduced in size to minimize the bare image processing time (inference). The two tasks of steering and collision probability prediction share all the residual layers in order to reduce the network complexity and the frame processing time. Then, two separate fully connected layers independently infer steering and collision probabilities. Mean-squared error (MSE) and binary cross-entropy (BCE) have been used to train the two predictions, respectively. A temporal dependent weighting of the two losses ensures the training convergence despite the different gradients’ magnitude produced by each loss. Eventually, to make the optimization focus on the samples that are most difficult to learn, hard negative mining was deployed in the final stages of learning. The two tasks have separate datasets to learn from. Steering angle prediction was trained with the *Udacity* dataset⁴, while the collision probability was trained with the *Zürich bicycle* dataset⁵.

The outputs of *DroNet* are used to command the UAV to move on a plane with forward velocity v_k and steering

² <https://www.tensorflow.org/lite>

³ <https://arm-software.github.io/ComputeLibrary>

⁴ <https://www.udacity.com/self-driving-car>

⁵ <http://rpg.ifi.uzh.ch/dronet.html>

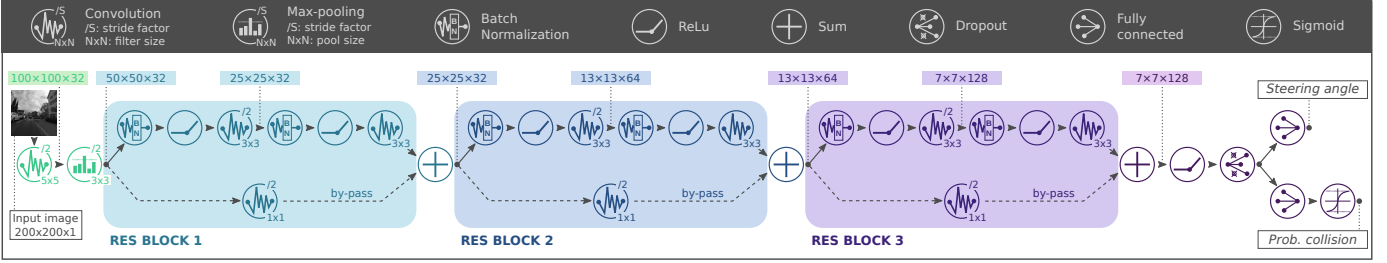


Fig. 2: DroNet [1] topology.

angle θ_k . More specifically, the low-pass filtered probability of collision is used to modulate the UAV forward velocity, while the low-pass filtered steering angle is converted to the drone’s yaw control. The result is a single relatively shallow network that processes all visual information and directly produces control commands for a flying drone. Learning the coupling between perception and control end-to-end provides several advantages, such as a simple, lightweight system and high generalization abilities. Indeed, the method was shown to function not only in urban environments but also on a set of new application spaces without any initial knowledge about them [1]. More specifically, even without a map of the environment, the approach generalizes very well to scenarios completely unseen at training time, including indoor corridors, parking lots, and high altitudes.

B. GAP8 Architecture

Our deployment target for the bulk of the DroNet computation is GAP8, a commercial embedded RISC-V multi-core processor derived from the PULP open source project⁶. At its heart, GAP8 is composed by an advanced RISC-V microcontroller unit coupled with a programmable octacore accelerator with RISC-V cores enhanced for digital signal processing and embedded deep inference.

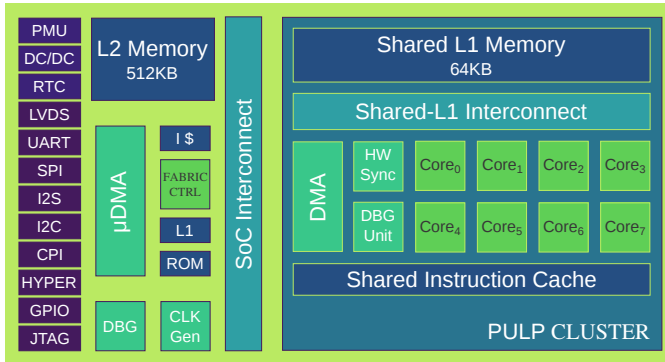


Fig. 3: Architecture of the GAP8 embedded processor.

Figure 3 shows the architecture of GAP8 in detail. The processor is composed by two separate power and clock domains, the FABRIC CTRL (FC) and the CLUSTER (CL). The FC is an advanced microcontroller unit featuring a single RISC-V core coupled with 512 kB of SRAM (*L2 memory*). The FC uses an in-order, DSP-extended four-stage microarchitecture

implementing the RISC-V instruction set architecture [31]. The core supports the RV32IMC instruction set consisting of the standard ALU instructions plus the multiply instruction, with the possibility to execute compressed code. In addition to this, the core is extended to include a register-register multiply-accumulate instruction, packed SIMD (single instruction multiple-data) DSP instructions (e.g. fixed-point dot product), bit manipulation instructions and two hardware loops. Moreover, the SoC features an autonomous multi-channel I/O DMA controller (μDMA) [32] capable of transferring data between a rich set of peripherals (QSPI, I2S, I2C, HyperBus, Camera Parallel Interface) and the L2 memory with no involvement of the FC. The HyperBus and QSPI interfaces can be used to connect GAP8 with an external DRAM or Flash memory, effectively extending the memory hierarchy with an external L3 having a bandwidth of 333 MB/s and capacity up to 128 Mbit. Finally, the GAP8 SoC also includes a DC/DC converter converting the battery voltage down to the required operating voltage directly on chip, as well as two separate frequency-locked loops (FLL) for ultra-low power clock generation [33].

The CLUSTER is dedicated to the acceleration of computationally intensive tasks. It contains eight RISC-V cores (identical to the one used in the FC) sharing a 64 kB multi-banked *shared L1 scratchpad memory* through a low-latency, high-throughput logarithmic interconnect [34]. The shared L1 memory supports single-cycle concurrent access from different cores requesting memory locations on separate banks and a starvation-free protocol in case of bank contentions (typically <10% on memory-intensive kernels). The eight cores are fed with instruction streams from a single shared, multi-ported I-cache to maximize the energy efficiency on data-parallel code. A cluster DMA controller is used to transfer data between the shared L1 scratchpad and the L2 memory; it is capable of 1D and 2D bulk memory transfer on the L2 side (only 1D on the L1 side). A dedicated *hardware synchronizer* is used to support fast event management and parallel thread dispatching/synchronization to enable ultra-fine grain parallelism on the cluster cores. CLUSTER and FABRIC CTRL share a single address space and communicate with one another by means of two 64-bit AXI ports, one per direction. A software runtime resident in the FC oversees all tasks offloaded to the CL and to the μDMA . On turn, a low-overhead runtime on the CL cores exploits the hardware synchronizer to implement shared-memory parallelism in the fashion of OpenMP [35].

⁶ <http://pulp-platform.org>

TABLE II: DroNet accuracy on PULP. In **bold** the configuration used for the final deployment.

Training			Inference - Fixed16					
Dataset	Max-Pooling	Data Type	Original Dataset				HiMax Dataset	
			EVA	RMSE	Accuracy	F1-score	Accuracy	F1-score
Original	3 × 3	Float32	0.758	0.109	0.952	0.888	0.859	0.752
	3 × 3	Fixed16	0.746	0.115	0.946	0.878	0.841	0.798
	2 × 2	Float32	0.766	0.105	0.945	0.875	0.845	0.712
	2 × 2	Fixed16	0.795	0.097	0.935	0.857	0.873	0.774
Original + HiMax	3 × 3	Float32	0.764	0.104	0.949	0.889	0.927	0.884
	3 × 3	Fixed16	0.762	0.109	0.956	0.894	0.918	0.870
	2 × 2	Float32	0.747	0.109	0.964	0.916	0.900	0.831
	2 × 2	Fixed16	0.732	0.110	0.977	0.946	0.891	0.821

IV. CNN MAPPING METHODOLOGY

In this section, we discuss and characterize the main methodological aspects related to the deployment of *DroNet* on top of the GAP8 embedded processor. This task showcases all the main challenges for a typical deep learning application running on resources-constrained embedded IoT node. Therefore, while our visual navigation engine is application-specific, the underlying methodology we present in the following of this section is general in nature and could be applied also to other resource-bound embedded systems where computationally intense tasks have to be performed under a real-time constraint on a parallel architecture.

A. Deploying *DroNet* on GAP8

Following an initial characterization phase, we calculated the original convolutional neural network (CNN) to involve ~ 41 MMAC operations per frame (accounting only for convolutional layers) and more than 1 MB of memory needed only to store the network’s weights, yielding a baseline for the amount of resources required on our navigation engine⁷. To successfully deploy the CNN on top of GAP8, the execution of *DroNet* has to fit within the strict real-time constraints dictated by the target application, while respecting the bounds imposed by the on-chip and on-board resources. Specifically, these constraints can be resumed in three main points:

- the *minimum real-time frame-rate* required to select a new trajectory on-the-fly or to detect a suspected obstacle in time to prevent a potential collision;
- the native *quality-of-results* must be maintained when using an embedded ultra-low power camera (in our prototype, the *HiMax* – see Section V for details) instead of the high resolution camera used by the original *DroNet*;
- the *amount of available memory* on the GAP8 SoC, where as reported in Section III-B we can rely on 512 kB of L2 SRAM and 64 kB of shared L1 scratchpad (TCDM), sets an upper bound to the size of operating set and dictates ad-hoc memory management strategy.

Therefore, it is clear there is a strong need for a strategy aimed at reducing the memory footprint and computational

load to more easily fit within the available resources, while exploiting the architectural parallelism at best to meet the real-time constraint. Therefore, the original *DroNet* network [1] has been modified to ease its final deployment; we operated incrementally on the model and training flow provided by the original *DroNet*, based on Keras/TensorFlow⁸.

The first change we performed is the reduction of the numerical representation of weights and activations from the native one, 32-bit floating point (Float32), down to a more economical and hardware-friendly 16-bit fixed point one (Fixed16) that is better suited for the deployment on any MUC-class processor without floating point unit (FPU), like in our GAP8 SoC. By analyzing the native Float32 network post-training, we determined that a dynamic range of ± 8 is sufficient to represent all weights and intermediate activations with realistic inputs. Accordingly, we selected a Fixed16 Q4.12 representation, using 4 bits for the integer part (including sign) and 12 bits for the fractionary part of both activations and weights (rounding down to a precision of 2^{-12}). Then, we retrained the network from scratch replacing the native convolutional layers from Keras to make them “quantization-aware”, using the methodology proposed by Hubara et al. [36].

The second significant change with respect to the original version of *DroNet* is the extension of the collision dataset used in [1] (named *Original* dataset) with ~ 1300 images (1122 for training and 228 for test/validation) acquired with the same camera that is available on-board the nano-drone (named *HiMax* dataset). Fine-tuning approaches, like dataset extension, have proved to be particularly effective at improving network generalization capability [37]. In our case, the original dataset is built starting from high-resolution color cameras whose images are significantly different from the ones acquired by the ULP low-resolution grayscale camera available in our navigation engine, particularly in terms of contrast. Therefore, we extended the training set and we evaluate our CNN for both datasets separately. Finally, we modified the receptive field of max-pooling layers from 3×3 to 2×2 , which yields essentially the same final results while reducing the execution time of max-pooling layers by $2.2 \times$ and simplifying their final implementation on GAP8.

Table II summarizes the results in terms of accuracy for all these changes. Explained Variance⁹ (EVA) and Root-Mean-

⁷ The baseline MMAC count does not correspond to the final implementation’s instruction count, because it does not account for implementation details such as data marshaling operations to feed the processing elements; however, it can be used to set an upper bound to the minimum execution performance that is necessary to deploy *DroNet* at a given target frame rate.

⁸ https://github.com/uzh-rpg/rpg_public_dronet

⁹
$$EVA = \frac{Var[y_{true} - y_{pred}]}{Var[y_{true}]}$$

Square Error (RMSE) refer to the regression problem (i.e., steering angle) whereas Accuracy and F1-score¹⁰ are related to the classification problem (i.e., collision probability), evaluated on both the *Original* and *HiMax* datasets. Regarding the *Original* dataset, it is clear that the proposed modifications are not penalizing the overall network’s capabilities. Moreover, fine-tuning increases performance for almost all cases (both regression and classification). Considering the test on the *HiMax* dataset, there is a clear improvement in term of collision accuracy when training is done with the extended dataset. In fact, if we consider paired configurations, the fine-tuned one based is always outperforming its counterpart, up to 8% in accuracy (i.e., max-pooling 3×3 , Fixed16). In Table II we also highlight (in bold) the scores achieved by the final version of *DroNet* deployed on GAP8.

B. AutoTiler

One of the biggest constraints in ULP embedded SoC’s without caches is the explicit management of the memory hierarchy; that is, how to marshal data between the bigger - and slower - memories and the smaller - but faster - ones tightly coupled to the processing elements. A common technique is *tiling* [38], which involves *i*) partitioning the input and output data spaces in portions or tiles small enough to fit within the smallest memory in the hierarchy (in our case, the shared L1) and *ii*) setting up an outer loop iterating on tiles, with each iteration comprising the loading of an input tile into the L1, the production of an output tile, and the storage of the output tile into the higher levels of the memory hierarchy. Tiling is particularly effective for algorithms like deep neural networks exposing very regular execution and data access patterns. As part of this work, we propose a tiling methodology that optimizes memory utilization on GAP8, while at the same time relieving the user from tedious and error-prone manual coding of the tiling loop and of the data movement mechanism.

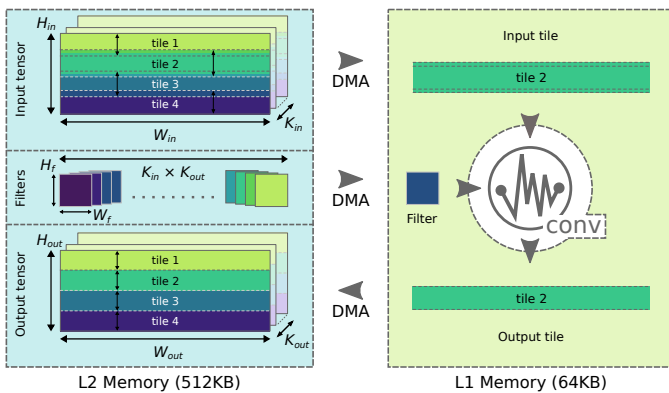


Fig. 4: Convolutional layer tiling.

Considering Figure 4 as a reference, each layer in a CNN operates on a three-dimensional input tensor representing a *feature space* (with one *feature map* per channel) and produces a new 3D tensor of activations as output. Convolutional layers, in particular, are composed of a linear transformation that maps K_{in} input feature maps into K_{out} output feature maps by

means of $K_{in} \times K_{out}$ convolutional filters (or weight matrices). Therefore, in any convolutional layer we can identify three different data spaces which can be partitioned in tiles in one or more of the three dimensions (i.e., W , H and K in Figure 4). Similar considerations can be made also for the other layers in a CNN, allowing to treat them in the same fashion.

As the design space defined by all possible tiling schemes is very large, we developed a tool called *AutoTiler* to help explore a subset of this space, choose an optimal tiling configuration, and produce C wrapping code that orchestrates the computation in a pipelined fashion as well as double-buffered memory transfers, taking advantage of the cluster DMA controller to efficiently move data between the L2 and L1 memories. The fundamental unit of computation assumed by the *AutoTiler* tool is the *basic kernel*, a function assuming that all its working data is already located in the L1 shared memory. Examples of basic kernels include convolution, max-pooling, ReLU rectification, addition. To map the overall high-level algorithm to a set of basic kernels that operate iteratively on tiles, the *AutoTiler* introduces a second level of abstraction: the *node kernel*. The structure of the target algorithm is coded by the developer as a dependency graph, where each node (a node kernel) is a composition of one or more basic kernels together with a specification of the related iteration space over W , H , K_{in} , K_{out} . For example, a node kernel for a convolutional layer can be composed of a first basic kernel for setting the initial bias, a central one to perform convolutions and a final one for ReLU rectification: in the *prologue*, *body* and *epilogue*, respectively. The *AutoTiler* treats the tiling of each node kernel as an independent optimization problem constrained by the node kernel specification and the memory sizes. This approach allows to build complex execution flows reusing hand-optimized *basic kernels* and abstracting the underneath complexity from the developer.

C. Tiling, Parallelization & Optimization

As introduced in Section III, the GAP8 SoC features 8+1 RISC-V cores with DSP-oriented extensions. To develop an optimized, high-performance and energy-efficient application for GAP8 and meet the required real-time constraint, it is paramount that the most computationally intense kernels of the algorithm are parallelized to take advantage of the 8-core cluster and are fully using the available specialized instructions. For the purpose of this work, we used the *AutoTiler* to fully implement the structure of the modified *DroNet*, therefore these optimization steps are reduced to hand-tuned parallelization and optimization of the basic kernels.

To exploit the available computational/memory resources at best, we constrain the *AutoTiler* to target the following general scheme: the input tensor is tiled along the H_{in} and K_{in} dimensions, while the output tensor is tiled along H_{out} and K_{out} ones. The stripes along H_{in} are partially overlapped with one another to take into account the receptive field of convolutional kernels at the tile border. Execution of the node kernel happens in either a *spatial* or *feature-wise* fashion, which differ in the ordering of the tiling loops and in the parallelization scheme that is applied. In the spatial scheme, work is split among parallel cores along the W_{out}

¹⁰ $F-1 = 2 \frac{precision \times recall}{precision + recall}$

Listing 1 Example of *spatial* execution scheme. x , w , y are the multi-dimensional input, weight and output tensors in L2 memory; \hat{x} , \hat{w} and \hat{y} are their respective tiles in L1 memory.

```

# weight DMA-in
DMA_Copy( $\hat{w} \leftarrow w$ )
for t in range(nb_tiles_H): # tiling over H
    # prologue operation (set bias value)
     $\hat{y} \leftarrow \text{BasicKernel\_SetBias}(\hat{y})$ 
    for j in range(nb_tiles_Kin): # tiling over  $K_{in}$ 
        # input tile DMA-in
        DMA_Copy( $\hat{x} \leftarrow x[j,t]$ )
        for i in range( $K_{out}$ ):
            # body operation (convolution)
             $\hat{y} \leftarrow \text{BasicKernel\_Conv\_Spatial}(\hat{y})$ 
         $\hat{y} \leftarrow \text{BasicKernel\_ReLU}(\hat{y})$ 
    # output tile DMA-out
    DMA_Copy( $y[i,t] \leftarrow \hat{y}$ )

```

Listing 2 Example of *feature-wise* execution scheme. x , w , y are the multi-dimensional input, weight and output tensors in L2 memory; \hat{x} , \hat{w} and \hat{y} are their respective tiles in L1 memory.

```

for i in range(nb_tiles_Kout): # tiling over  $K_{out}$ 
    # weight DMA-in
    DMA_Copy( $\hat{w} \leftarrow w[i]$ )
    # prologue operation (set bias value)
     $\hat{y} \leftarrow \text{BasicKernel\_SetBias}(\hat{y})$ 
    for j in range(nb_tiles_Kin): # tiling over  $K_{in}$ 
        # input tile DMA-in
        DMA_Copy( $\hat{x} \leftarrow x[j]$ )
        # body operation (convolution)
         $\hat{y} \leftarrow \text{BasicKernel\_Conv\_FeatWise}(\hat{w}, \hat{x}, \hat{y})$ 
    # epilogue operation (ReLU)
     $\hat{y} \leftarrow \text{BasicKernel\_ReLU}(\hat{y})$ 
    # output tile DMA-out
    DMA_Copy( $y[i] \leftarrow \hat{y}$ )

```

dimension; Figure 4 and 5-A refer to this scheme, which is also exemplified in Listing 1. In the feature-wise scheme, which we only apply on full feature maps (i.e. the number of tiles in the H_{out} direction is 1), work is split among cores along the K_{out} dimension; this scheme is shown in Figure 5-B and Listing 2. The choice of one scheme over the other is influenced mostly by the parallelization efficiency: after an exploration phase, we found the best performance arised when using the spatial scheme for the first node kernel of *DroNet* (first convolution + max-pooling), while using the feature-wise approach for the rest. This choice is related to the fact that in deeper layers the feature map size drops rapidly and the spatial scheme becomes suboptimal, because the width of each stripe turns too small to achieve full utilization of the cores.

To further optimize the *DroNet* execution, we made use of all the optimized signal processing instructions available in GAP8. These include packed-SIMD instructions capable of exploiting sub-word parallelism, as well as bit-level manipulation and shuffling, which can be accessed by means of compiler intrinsics such as `__builtin_pulp_dotsp2` (for 16-bit dot product with 32-bit accumulation), `__builtin_shuffle` (permutation of elements within two input vectors), `__builtin_pulp_pack2` (packing two scalars into a vector).

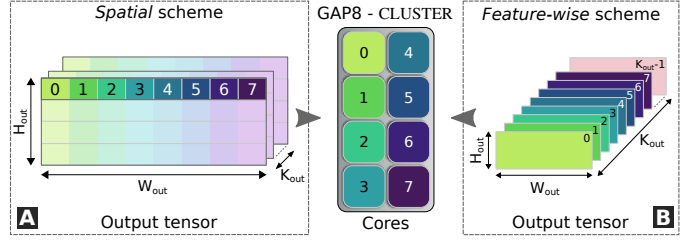


Fig. 5: Parallelization schemes utilized in the *DroNet* layers for deployment on GAP8; the different colors represent allocation to a different core.

D. L2 Memory Management Strategy

Given *i*) the residual-network topology of *DroNet*, which requires to increase the lifetime of the output tensors of some of the layers (due to bypass layers), and *ii*) the “scarcity” of L2 memory as a resource to store all weights and temporary feature maps (we would need more than 1MB in view of 512kB available), an ad-hoc memory management strategy for the L2 memory is required, similar to what is done between L2 and L1 using the GAP8 *AutoTiler*. Due to the high energy cost of data transfers between L3 and L2, the strategy needs to be aimed at the maximization of the L2 reuse.

At boot time, before the actual computation loop starts, *i*) we load all the weights, stored in the external flash memory as binary files, in the L3 DRAM memory and *ii*) we call from the fabric controller the *runtime* allocator to reserve two L2 *allocation stacks* (shown in Figure 7) where intermediate buffers will be allocated and deallocated in a linear fashion. The choice to use two allocation stacks instead of a single one is due to the fact that in the latter case, we would need to keep alive up to 665 kB in L2 due to data dependencies, which is more than the available space. Our allocation strategy simply updates the pointer of the next free location in the pre-allocated L2 stack, avoiding the runtime overhead of library allocation/free functions. We differentiate our strategy between weights and feature maps: for the former, we allocate space just before their related layer and deallocate it just after the layer execution, as also shown in the pseudo-code blocks of Figure 6. For the latter, due to the residual network bypasses, we often have to prolongate the lifetime of a feature map during the execution of the two following layers (node kernels in Figure 6). Therefore, for each RES block there will be an amount of time where 3 tensors have to be stored at the same time.

Figure 6 shows the full execution flow of *DroNet* related to our solution, annotated with the sequence of node kernels and the L3/L2 memory management blocks. For the sake of readability, in Figure 6, we report only the first RES block, but this can be generalized also to the others with few minor modifications and updating input, output and weights id. In the pseudo-code of Figure 6 the second parameter of the `Alloc` and `Free` function specifies the allocation buffer (i.e., Allocation stack 0 or Allocation stack 1 in Figure 7). Note that, the μ DMA copies the weights from L3 to L2 just after the destination L2 area is allocated. The buffers’ memory allocation sequence is reported in Figure 7

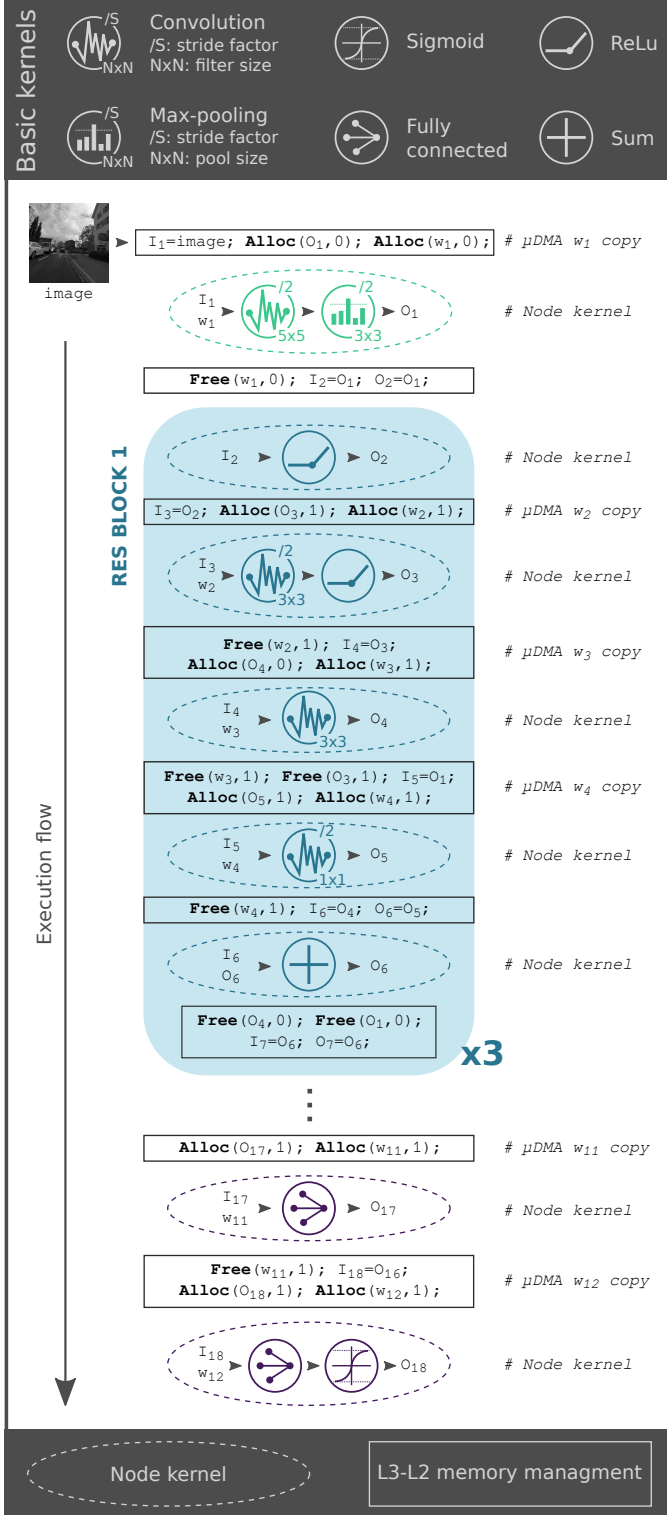


Fig. 6: *DroNet* on PULP execution graph (with pseudo-code).

(from left to right) for the entire *DroNet* execution. The columns of the two stacks represent the data needed at each execution step, where O_i and w_j represent the input/output feature maps and weights, respectively. The last row of each stack reports the total amount of L2 memory required at each step. Thus, the final dimension of each stack is given by the column with the biggest occupancy (highlighted in light blue

Allocation stack 0							
$O_1 \rightarrow O_1$	$O_8 \rightarrow O_8$	$O_{10} \rightarrow O_{10}$					
w_1	O_4	w_5	w_6	w_7	w_8	w_9	O_{15}
162kB	200kB	59kB	96kB	26kB	169kB	308kB	26kB

Allocation stack 1							
$O_3 \rightarrow O_3$	$O_5 \rightarrow O_5$	$O_{13} \rightarrow O_{13}$	$O_{13} \rightarrow O_{13}$	$O_{13} \rightarrow O_{13}$	$O_{17} \rightarrow O_{17}$	$O_{17} \rightarrow O_{17}$	$O_{17} \rightarrow O_{17}$
w_2	w_3	w_4	O_9	$O_{14} \rightarrow O_{14}$	w_9	w_9	w_9
58kB	58kB	42kB	62kB	26kB	42kB	13kB	13kB

Fig. 7: L2 memory allocation sequence.

in Figure 7), resulting in 370 kB of L2 memory. Therefore, our solution not only allows to the *DroNet* execution within the L2 memory budget constraint but results in leaving 142 kB of the L2 still available (i.e., $\sim 28\%$ of the total) for additional on-board tasks like target following [39], etc.

V. THE PULP-SHIELD

To host our visual navigation algorithm we designed a lightweight, modular and configurable printed circuit board (PCB) with highly optimized layout and a form factor compatible to our nano-size quadrotor. It features a PULP-based GAP8 SoC, two Cypress *HyperBus Memories*¹¹ and an ultra-low power *HiMax* CMOS image sensor¹² able to run up to 60 fps with a gray-scale resolution of 320×240 pixels with just 4.5 mW of power. Our pluggable PCB, named *PULP-Shield*, has been designed to be compatible with the *Crazyflie 2.0* (CF) nano-quadrotor¹³. This vehicle has been chosen due to its reduced size (i.e., 27 g of weight and 10 cm of diameter) and its open-source and open-hardware philosophy. The communication between the PULP chip and the main MCU on-board the nano-drone (i.e., *ST Microelectronics STM32F405*¹⁴) is realized via a SPI interface and two GPIO signals.

In Figure 8 the schematic of the proposed *PULP-Shield* is shown. Two BGA memory slots allow all possible combinations of *HyperRAM*, *HyperFlash* and hybrid *HyperFlash/RAM* memory packages. In this way we can select the most appropriate memory configuration given a target application. We mounted on one slot a 64 Mbit *HyperRAM* (DRAM) chip and on the other a 128 Mbit *HyperFlash* memory, embodying the system L3 and the external storage, respectively.

On the PCB (Figure 8-B) there is also a camera connector that allows the *HiMax* camera to communicate with the rest of the system through the parallel camera interface (PCI) protocol. Two mounting holes, on the side of the camera connector, allow to plug a 3D-printed camera holder that can be set either in front-looking or down-looking configuration. Those two configurations are representative of the most common visual sensors layouts typically embedded in any autonomous flying vehicles. In fact, the front-looking configuration can be used

¹¹ <http://www.cypress.com/products/hyperbus-memory>

¹² <http://www.himax.com.tw/products/cmos-image-sensor/image-sensors>

¹³ <https://www.bitcraze.io/crazyflie-2>

¹⁴ <http://www.st.com/en/microcontrollers/stm32f405-415.html>

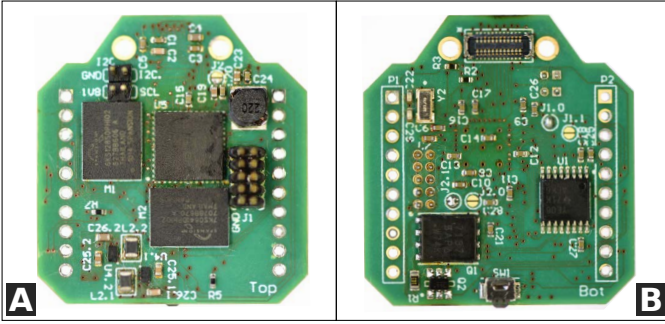


Fig. 8: The *PULP-Shield* pluggable PCB. Top view (A) and bottom view (B).

for many navigation tasks like path planning [40], obstacle avoidance [41], trajectory optimization [8], just to name a few. Instead, the down-looking camera configuration is usually chosen for stabilization tasks like distance estimation [42], way-point tracking and positioning [43], etc.

On the shield there are also a JTAG connector for debug purposes and an external I2C plug for future development. Two headers, located on both sides of the PCB, grant a steady physical connection with the drone and at the same time they bring the shield power supply and allow communication with the CF through the GPIOs and the SPI interface. The form factor of our final *PULP-Shield* prototype is 30×28 mm and it weighs ~ 5 g (including all components), well below the payload limit imposed by the nano-quadcopter.

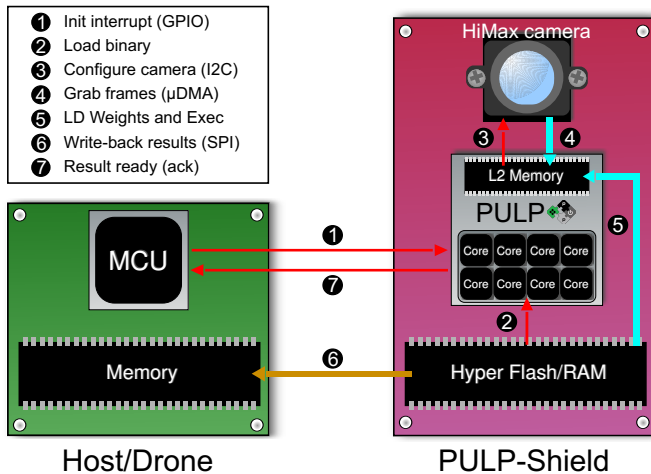


Fig. 9: Example of interaction between the *PULP-Shield* and the drone.

Similarly to what has been presented in [35], the *PULP-Shield* embodies the *Host-Accelerator* architectural paradigm, where the CF’s MCU offloads the intensive visual navigation workload to the PULP accelerator. As depicted in Figure 9 the interaction starts from the host, which wakes up the accelerator with a GPIO interrupt ①. Then, the accelerator fetches from its external *HyperFlash* storage the kernel (stored as binary file) to be executed: *DroNet* in our case ②. Note that, in this first part of the protocol the host can also specify which kernel should be executed, as well as a sequence of several pre-loaded kernels available on the external Flash storage. At this point,

the GAP8 SoC can configure the *HiMax* camera via an internal I2C ③ and start to transfer the frames from the sensor to the L2 shared memory through the μ DMA ④. All additional data, like the weights used in our CNN, can be loaded from the DRAM/Flash memory and parallel execution is started on the accelerator ⑤. Lastly, the results of the computation are returned to the drone’s MCU via SPI ⑥ and the same host is acknowledged about the available results with a final interrupt over GPIO ⑦. Note that, the transfer of a new frame is performed by the μ DMA overlapping the CNN computation on the previous frame performed in the CLUSTER.

Even if the *PULP-shield* has been developed specifically to fit the CF quadcopter, its basic concept and the functionality it provides are quite general, and portable to any drone based on an SPI-equipped MCU and more generally to generic IoT nodes requiring visual processing capabilities. The system-level architectural template it is based on is meant for minimizing data transfers (i.e., exploiting locality of data) and communication overhead between the main MCU and the accelerator – without depending on the internal microarchitecture of either one.

VI. EXPERIMENTAL RESULTS

In this section we present the experimental evaluation of our visual navigation engine, considering three main metrics: *i)* the capability of respecting a given real-time deadline, *ii)* the capability of performing all the required computations within the allowed power budget and *iii)* the final accuracy of the closed-loop control, given as reaction time w.r.t. an unexpected obstacle. All the results are based on the *PULP-shield* configuration presented in Section V.

A. Performance & Power Consumption

We measured wall-time performance and power consumption by sweeping between several operating modes on GAP8. We focused on operating at the lowest (1.0 V) and highest (1.2 V) supported core VDD voltages. We swept the operating frequency between 50 and 250 MHz, well beyond the GAP8 officially supported configuration¹⁵. Figure 10 provides a complete view of the power consumption in all experimentally possible operating modes of GAP8 on the *DroNet* application while sweeping both FABRIC CTRL (FC) and CLUSTER (CL) clock frequency, both at 1.0 V and 1.2 V, and the related achievable frame-rate. Figure 10-A shows the energy-efficiency of all available configurations as heat map, where the most energy efficient one is represented by VDD@1.0 V, FC@50 MHz and CL@100 MHz. In Figure 10-B1 we report performance as frame-rate and total power consumption measured before the internal DC/DC converter utilized on the SoC. Selecting a VDD operating point of 1.2 V would increase both power and performance up to 272 mW and 18 fps. We found the SoC to be working correctly @ 1.0 V for frequencies up to ~ 175 MHz; we note that as expected when operating @ 1.0 V there is a definite advantage in terms of energy efficiency. Therefore, for the sake of readability, in Figure 10 we avoid to show configurations of VDD 1.2 V that

¹⁵ <https://greenwaves-technologies.com/gap8-datasheet>

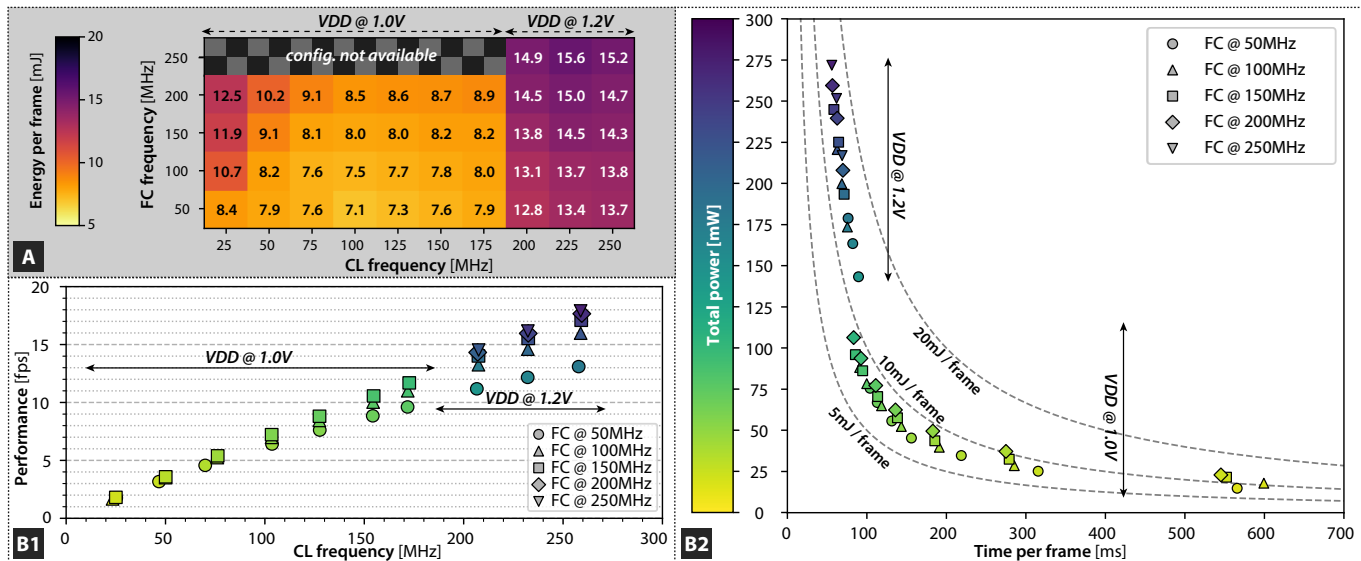


Fig. 10: A) Heat map showing the energy per frame in all tested configurations of GAP8 with VDD@1.0 V and VDD@1.2 V; B1) *DroNet* performance in frames per second (fps) in all tested configurations (coloring is proportional to total system power); B2) *DroNet* total system power vs time per frame in all tested configurations; dashed gray lines show the levels of energy efficiency in mJ/frame.

would reach same performance of VDD 1.0 V at higher cost in term of power. Similarly, in Figure 10-B2 we report power consumption vs time to compute one frame.

TABLE III: Power consumption & Execution time per frame of *DroNet* on GAP8 VDD@1.0 V, FC@50 MHz, CL@100 MHz.

Layer	AVG Power [mW]	Exec Time [ms]	L3-L2 Time [ms]
conv_1 + pool	47.1	22.6	0.1
ReLU	24.8	0.9	—
conv_2 + ReLU	38.7	17.3	0.6
conv_3	38.0	14.3	0.6
conv_4	43.6	7.3	0.1
add	38.9	0.3	—
ReLU	27.6	0.2	—
conv_5 + ReLU	37.7	9.3	1.2
conv_6	34.8	17.0	2.4
conv_7	32.7	4.2	0.2
add	24.3	0.3	—
ReLU	20.5	0.3	—
conv_8 + ReLU	33.1	13.0	4.7
conv_9	31.9	24.8	9.4
conv_10	41.9	5.4	0.5
add + ReLU	24.4	0.3	—
fully_1	13.0	0.1	0.4
fully_2	13.0	0.1	0.4

In Figure 11 we present the power traces for a full end-to-end execution of *DroNet*, measured using a bench DC power analyzer¹⁶. The power traces are measured by powering the GAP8 SoC, with the most energy-efficient configuration at 1.0 V core voltage and operating at 50 MHz on FC and 100 MHz on CL. The detailed average power consumption (including both the FC and CL domains) is reported in

Table III. The peak power consumption of 47 mW is associated to the 1st convolutional layer; we used this value to compute the overall power envelope of our node. Instead, the minimum power consumption is given by the two last fully connected layers consuming 13 mW each. The average power consumption, weighted over the duration of each layer, is 39 mW, which grows to 45 mW including also the losses on the internal DC/DC converter (not included in Figure 11). In the full *DroNet* execution, layers are interposed with L3-L2 data transfers, happening with the CL cores in clock-gated state, which account for $\sim 7\%$ of the overall execution time. Therefore, power consumption for the entire board settles to 64 mW if we consider also the cost of L3 memory access and the on-board ULP camera.

In Figure 12 is reported the power break-down for the complete cyberphysical system and for proposed *PULP-Shield*. Our nano-quadcopter is equipped with a 240 mA h 3.7 V LiPo battery enabling a flight time of 7 minutes under standard conditions, which results in an average power consumption of 7.6 W. The power consumption of all the electronics on-board of the original drone amounts to 277 mW leaving ~ 7.3 W for the 4 rotors. The electronics consumption is given by the 2 MCUs included in the quadrotor and all the additional devices (e.g., sensors, leds, etc.). In addition to that, introducing the *PULP-Shield*, we increase the peak power envelope by 64 mW using the most energy-efficient configuration and by 284 mW selecting the fastest configuration (0.8% and 3.5% of the total, respectively). On the *PULP-Shield* we consider the HyperRAM operating at full speed only for the time required for L3-L2 data transfers (as shown in Table III) with an average power consumption of 8 mW for the fastest configuration, as reported in Figure 12-B. Notice that this is a worst-case figure, taking account of both the GAP8 SoC and the HyperRAM operating at full speed simultaneously.

¹⁶ www.keysight.com/en/pd-1842303-pn-N6705B

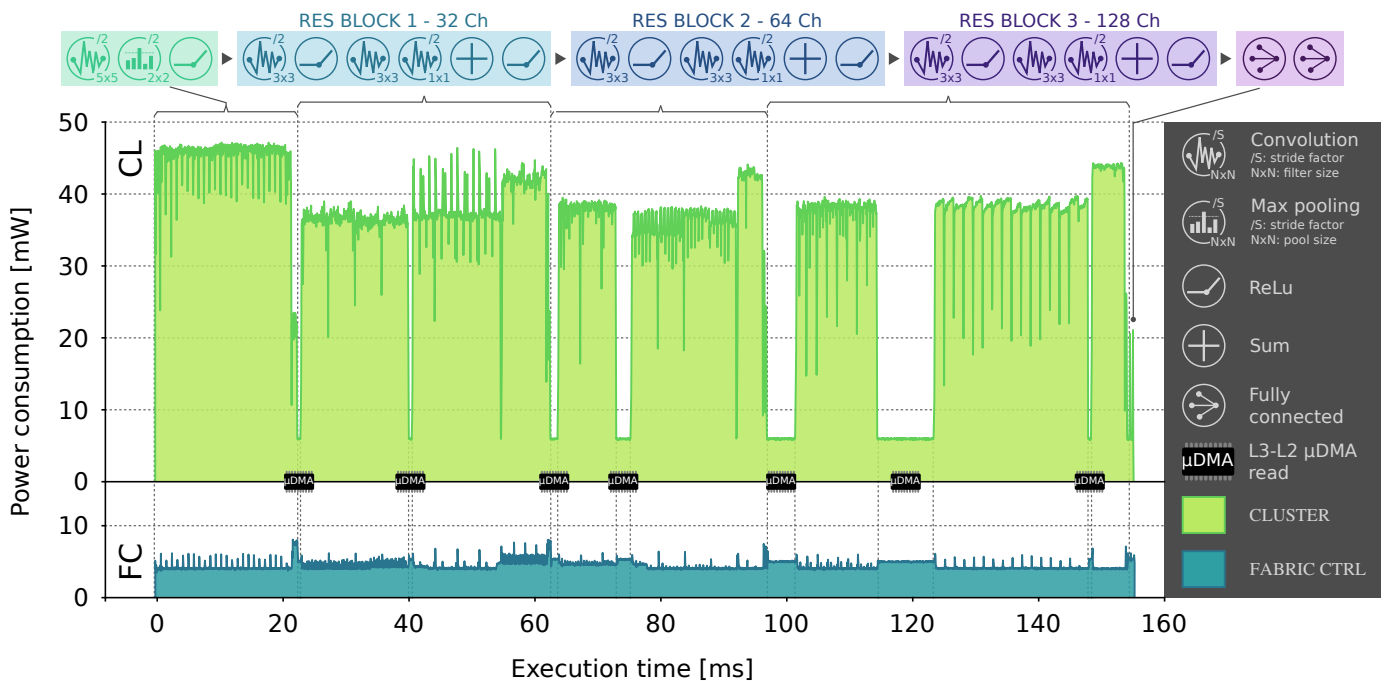


Fig. 11: Power traces per layer of *DroNet*, measured at VDD@1.0 V, FC@50 MHz, CL@100 MHz. The symbols on top of the plot indicate the computation stage associated to each visible phase in the power trace. Measurements are taken after internal DC/DC converter (i.e., accounting for both FABRIC CTRL and CLUSTER).

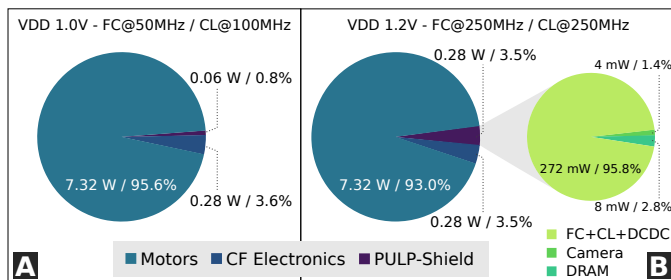


Fig. 12: Power envelope break-down of the entire cyberphysical system running at FC@50 MHz-CL@100 MHz (A) and FC@250 MHz-CL@250 MHz (B) with *PULP-Shield* zoom-in (on the right).

The power break-down of our visual navigation module can be seen on the right of Figure 12-B, where we include the computational unit, the L3 external DRAM memory and the ultra-low power camera. As on-board computation accounts for roughly 5% of the overall power consumption (propellers, sensors, compute and control, *cfr* Section I), our *PULP-Shield* enables the execution of the *DroNet* network (and potentially more) in all configurations within the given power envelope.

Finally, we performed an experiment to evaluate the cost in terms of operating lifetime of carrying the physical payload of the *PULP-Shield* and of executing the *DroNet* workload. To ensure a fair measurement, we decoupled the *DroNet* output from the nano-drone control and statically set it to *hover* (i.e., keep constant position over time) at 0.5 m from the ground. We targeted three different configurations: *i*) the original *CrazyFlie* (CF) without any *PULP-Shield*; *ii*) *PULP-Shield* plugged but never turned on, to evaluate the lifetime reduction due to the

additional weight introduced; *iii*) *PULP-Shield* turned on and execute *DroNet* at VDD@1.0 V, FC@50 MHz, CL@100 MHz. Our results are summarized in Table IV, where as expected the biggest reduction in lifetime is given by the increased weight. Ultimately, the price for our visual navigation engine is $\sim 22\%$ of the original lifetime.

TABLE IV: *CrazyFlie* (CF) lifetime with and without *PULP-Shield* (both turned off and running *DroNet* at VDD@1.0 V, FC@50 MHz, CL@100 MHz).

	Original CF	CF + <i>PULP-Shield</i> (off)	CF + <i>PULP-Shield</i> (on)
Lifetime	~ 440 s	~ 350 s	~ 340 s

B. State-of-the-Art Comparison & Discussion

To compare and validate our experimental results with respect to the current state-of-the-art, we targeted the most efficient CNN implementation currently available for micro-controllers, namely CMSIS-NN [27]. At peak performance in a synthetic test, this fully optimized library is able to achieve as much as 0.69 MAC/cycle on convolutions, operating on *Fixed8* data that is internally converted to *Fixed16* in the inner loop.

By contrast, we operate directly on *Fixed16* and achieve a peak performance of 0.64 MAC/cycle/core in a similar scenario (on the 6th layer of *DroNet*, 3 \times 3 convolution). The bypasses and the final layers are a bit less efficient, yielding an overall weighted peak throughput of 0.53 MAC/cycle/core on convolutional layers, which constitute the vast majority of the execution time.

In Table V we report the execution breakdown per frame for all activities performed by our CNN. We can see how

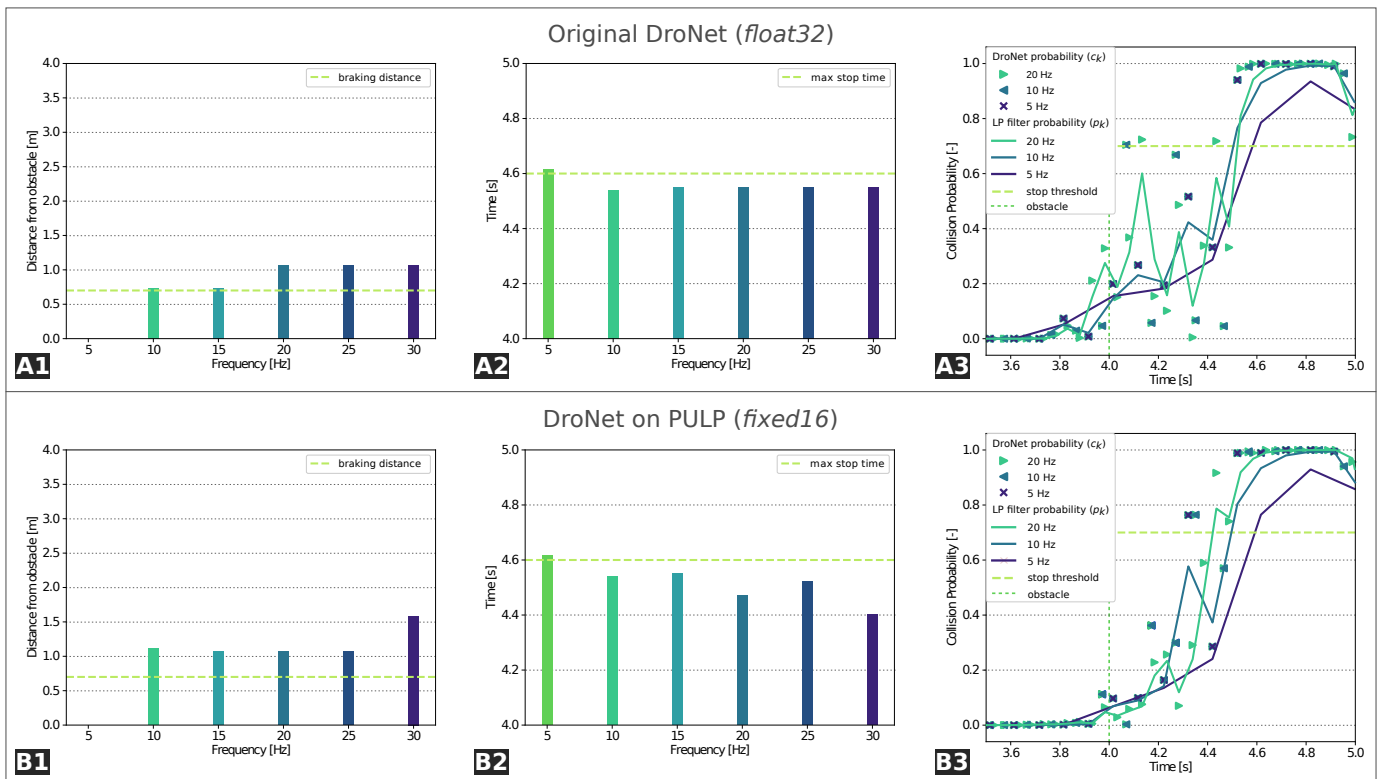


Fig. 13: Performance comparison between the original (A1-3) and quantized (B1-3) *DroNet* architectures. Stop command time (A1 and B1), minimum distance from obstacle (A2 and B2) and collision probability as output of both CNN and low-pass filter (A3 and B3).

TABLE V: CLUSTER-cycle break-down for processing one frame on the GAP8, both FC and CL @ 50 MHz

	μ DMA L3/L2	DMA L2/L1	Computation	Total
Cycles	1.03 M	0.11 M	13.47 M	14.61 M

the L3-L2 transfers (not overlapped to computation) and the non-overlappable part of L2-L1 transfers account for ~ 1.14 Mcycles of the overall execution time. Then, considering ~ 41 MMAC for the original CNN, in the ideal peak-throughput case of 4.28 MAC/cycle we would need ~ 10 Mcycles for computing one frame, instead of our measured 13.47 Mcycles. The overhead is due to inevitable non-idealities such as sub-optimal load balancing in layers exposing limited spatial parallelism as well as tiling control loops and the marshaling stage required by padded convolutions. Considering all of the aforementioned effects (i.e. computation non-idealities as well as memory transfers), we achieve a real throughput of 2.81 MAC/cycle in the *DroNet* execution – still $4\times$ better than the CMSIS-NN peak performance.

To further concretize the comparison, we take as an example target a top-notch high-performance microcontroller: a STM32H7¹⁷ sporting a Cortex-M7 core and capable of operating at up to 400 MHz. Without considering any data movement overhead, and taking into account only peak performance, this would be able to achieve up to 276 MMAC/s @ 346 mW. By comparison, our system can achieve an average

performance of 281 MMAC/s with the most power efficient configuration @ 45 mW, i.e. same performance within a $5.4\times$ smaller power budget. Moreover, if we consider our peak-throughput configuration (where both FC and CL are running @ 250 MHz) we can deliver up to 702 MMAC/s @ 272 mW: $2.5\times$ better with 21% less power. Even if it was possible to linearly up-scale the performance of this microcontroller to the same level of our system, it would consume ~ 880 mW, which would constitute largely more than the 5% of power envelope typically dedicated to on-board computation on nano-UAV systems [13]. This confirms that the parallel-ultra-low power approach adopted in our visual navigation engine significantly outperforms sequential processing in terms of energy efficiency, without compromising programmability and flexibility.

C. Control Accuracy

To fully exploit the intrinsic inertial agility of a lightweight nano-quadrotor as the *Crazyflie 2.0* used in our prototype, fast on-board perception is required. To evaluate the agility of our integrated system, we perform an experiment in which our flying platform is required to react to a sudden obstacle occluding its way. With this experiment we aim to demonstrate that the *PULP-Shield* computational resources are enough to make full use of the platform agility. As mentioned in Section IV-A, for the final deployment of *DroNet* on the *PULP-Shield*, we select the network trained with `Fixed16` quantization, 2×2 max-pool receptive field, and fine-tuning dataset. The choice is justified by both the quantization requirement of the GAP8

¹⁷ <http://www.st.com/en/microcontrollers/stm32h7-series.html>

SoC and the model performance, superior to other viable alternatives (see Table II).

The experimental setting is as follows: we collect a dataset of images by manually flying the drone over a straight path of 20 m at an average speed of 4 m s^{-1} . At the beginning of the test, the path is completely free from obstacles. At $T = 4 \text{ s}$ after the start of the experiment, an obstacle appears at the end of the track, leaving 4 m free for braking and stopping. The system is then required to raise a stop signal soon enough to avoid collision. As we show in the supplementary video, our integrated system has the capability to control the nano-drone in closed-loop. However, for safety reasons and to avoid damaging the platform, we don't control the nano-drone in closed-loop during this experiment. Instead, we process the frames collected with manual flight offline. The collected dataset is used to study the relation between the system operational frequencies and the drone's reaction time.

As in the original implementation of [1], network's predictions are low-pass filtered to decrease high-frequency noise. In detail, the collision probability p_k is a low-pass filtered version of the raw network output c_k ($\alpha = 0.7$):

$$p_k = (1 - \alpha)p_{k-1} + \alpha c_k, \quad (1)$$

Figure 13 (A3-B3) illustrates the predicted collision probability of the original and quantized *DroNet* CNN as a function of time. In the plots, we show both c_k and p_k at different frequencies, the former reported as markers, whereas the latter is shown as continuous line. An horizontal dashed orange line shows the threshold for sending a stop signal to the control loop ($p_k > 0.7$), instead a vertical red dashed line highlights the time at which the obstacle becomes visible ($T = 4 \text{ s}$).

In order to quantitatively evaluate the performance of our system at different operational frequencies, we computed the maximum time and the minimum distance from the object at which the stop command should be given to avoid collision. We deployed the *Crazyflie 2.0* parameters from [44] and the classical quadrotor motion model from [45] to *analytically* compute those two quantities. From this analysis, we derived a minimum stopping time of 400 ms and a braking distance of 0.7 m, assuming the platform moves with a speed of 4 m/s when it detects the obstacle.

In Figure 13 (A1-2, B1-2) we illustrate a performance comparison between our quantized system and the original implementation of [1]. Despite quantization, our network outperforms [1] in term of collision detection, and can react quicker to sudden obstacles even at low operational frequencies. This is in accordance to the results of Table II, and mainly due to the fine-tuning of our network to the *HiMax* camera images.

Both the quantized and original architecture share however a similar behaviour at different operational frequencies. More specifically, both fail to detect obstacles at very low frequencies (i.e., 5 Hz), but successfully avoid collision at higher frequencies. Interestingly, increasing the system frequencies does not always improve performance. This can be observed in Figure 13-B2, where performance at 20 Hz is better than at 25 Hz. from Figure 13 we can observe that inference at 10 Hz allows the drone to brake in time and avoid collision. This

confirm that our system, processing up to 18 fps, can *i)* make use of the agility of the *Crazyflie 2.0* and *ii)* be deployed in the same way as the original method to navigate in indoor/outdoor environments while avoiding dynamic obstacles.

VII. CONCLUSION

Nano- and pico-sized UAVs are ideal IoT nodes; due to their size and physical footprint, they can act as mobile IoT hubs, smart sensors and data collectors for tasks such as surveillance, inspection etc. However, to be able to perform these tasks, they must be capable of autonomous navigation of environments such as urban streets, industrial facilities and other hazardous or otherwise challenging areas. In this work, we present a complete deployment methodology targeted at enabling execution of complex deep learning algorithms directly on-board of resource-constrained milliwatt-scale nodes. We provide the first (to the best of our knowledge) completely vertically integrated hardware/software visual navigation engine for autonomous nano-UAVs with completely on-board computation – and thus potentially able to operate in conditions in which the latency or the additional power cost of a wirelessly-connected centralized solution.

Our system, based on a *GreenWaves Technologies* GAP8 SoC used as an accelerator coupled with the STM32 MCU on the *CrazyFlie 2.0* nano-UAV, supports real-time computation of *DroNet*, an advanced CNN-based autonomous navigation algorithm. Experimental results show a performance of 6 fps @ 64 mW selecting the most energy-efficient SoC configuration, that can scale up to 18 fps within an average power budget for computation of 284 mW. This is achieved without quality-of-results loss with respect to the baseline system on which *DroNet* was deployed: a COTS standard-size UAV connected with a remote PC, on which the CNN was running at 20 fps. Our results show that both systems are able to detect obstacles fast enough to be able to safely fly at high speed, 4 m/s in the case of the *CrazyFlie 2.0*. Overall, our contribution paves the way for a huge number of advanced use-cases of autonomous nano-UAVs as IoT-connected mobile smart sensors.

ACKNOWLEDGMENTS

The authors thank Hanna Müller for her contribution in designing the *PULP-Shield* and Noé Brun for his support in making the camera-holder.

REFERENCES

- [1] A. Loquercio, A. I. Maqueda, C. R. del Blanco, and D. Scaramuzza, "Dronet: Learning to fly by driving," *IEEE Robotics and Automation Letters*, vol. 3, no. 2, April 2018.
- [2] N. H. Motlagh, T. Taleb, and O. Arouk, "Low-altitude unmanned aerial vehicles-based internet of things services: Comprehensive survey and future perspectives," *IEEE Internet of Things Journal*, vol. 3, no. 6, Dec 2016.
- [3] F. Conti, R. Schilling, P. D. Schiavone, A. Pullini, D. Rossi, F. K. Gürkaynak, M. Muehlberghuber, M. Gautschi, I. Loi, G. Haugou, S. Mangard, and L. Benini, "An IoT Endpoint System-on-Chip for Secure and Energy-Efficient Near-Sensor Analytics," *IEEE Transactions on Circuits and Systems I: Regular Papers*, vol. 64, no. 9, pp. 2481–2494, Sep. 2017.
- [4] D. Palossi, A. Gomez, S. Draskovic, A. Marongiu, L. Thiele, and L. Benini, "Extending the lifetime of nano-blimps via dynamic motor control," *Journal of Signal Processing Systems*, Feb 2018.

- [5] D. Floreano and R. J. Wood, "Science, technology and the future of small autonomous drones," *Nature*, vol. 521, no. 7553, pp. 460–466, may 2015.
- [6] M. Piccoli and M. Yim, "Piccolissimo: The smallest micro aerial vehicle," in *2017 IEEE International Conference on Robotics and Automation (ICRA)*. IEEE, may 2017.
- [7] Y. Lin, F. Gao, T. Qin, W. Gao, T. Liu, W. Wu, Z. Yang, and S. Shen, "Autonomous aerial navigation using monocular visual-inertial fusion," *Journal of Field Robotics*, vol. 35, no. 1, pp. 23–51, jul 2017.
- [8] D. Falanga, E. Mueggler, M. Faessler, and D. Scaramuzza, "Aggressive quadrotor flight through narrow gaps with onboard sensing and computing using active vision," in *2017 IEEE International Conference on Robotics and Automation (ICRA)*, May 2017.
- [9] G. Loianno, D. Scaramuzza, and V. Kumar, "Special issue on high-speed vision-based autonomous navigation of uavs," *Journal of Field Robotics*, vol. 35, no. 1, pp. 3–4, 2018.
- [10] Y. Yang, Z. Zheng, K. Bian, L. Song, and Z. Han, "Real-time profiling of fine-grained air quality index distribution using uav sensing," *IEEE Internet of Things Journal*, vol. 5, no. 1, Feb 2018.
- [11] J. Conroy, G. Gremillion, B. Ranganathan, and J. S. Humbert, "Implementation of wide-field integration of optic flow for autonomous quadrotor navigation," *Autonomous robots*, vol. 27, no. 3, 2009.
- [12] K. McGuire, G. de Croon, C. D. Wagter, K. Tuyls, and H. Kappen, "Efficient optical flow and stereo vision for velocity estimation and obstacle avoidance on an autonomous pocket drone," *IEEE Robotics and Automation Letters*, vol. 2, no. 2, April 2017.
- [13] R. J. Wood, B. Finio, M. Karpelson, K. Ma, N. O. Pérez-Arancibia, P. S. Sreetharan, H. Tanaka, and J. P. Whitney, *Progress on "Pico" Air Vehicles*. Cham: Springer International Publishing, 2017.
- [14] S. Scherer, J. Rehder, S. Achar, H. Cover, A. Chambers, S. Nuske, and S. Singh, "River mapping from a flying robot: state estimation, river detection, and obstacle mapping," *Autonomous Robots*, vol. 33, no. 1-2, 2012.
- [15] D. Scaramuzza, M. C. Achtelik, L. Doitsidis, F. Friedrich, E. Kosmatopoulos, A. Martinelli, M. W. Achtelik, M. Chli, S. Chatzichristofis, L. Kneip, D. Gurdan, L. Heng, G. H. Lee, S. Lynen, M. Pollefeys, A. Renzaglia, R. Siegwart, J. C. Stumpf, P. Tanskanen, C. Troiani, S. Weiss, and L. Meier, "Vision-controlled micro flying robots: From system design to autonomous navigation and mapping in GPS-denied environments," *IEEE Robotics & Automation Magazine*, vol. 21, no. 3, pp. 26–40, sep 2014.
- [16] D. Gandhi, L. Pinto, and A. Gupta, "Learning to fly by crashing," in *2017 IEEE/RSJ International Conference on Intelligent Robots and Systems (IROS)*, sep 2017.
- [17] F. Sadeghi and S. Levine, "CAD2rl: Real single-image flight without a single real image," in *Robotics: Science and Systems XIII*, jul 2017.
- [18] N. Smolyanskiy, A. Kamenev, J. Smith, and S. Birchfield, "Toward low-flying autonomous mav trail navigation using deep neural networks for environmental awareness," in *2017 IEEE/RSJ International Conference on Intelligent Robots and Systems (IROS)*, Sept 2017.
- [19] S. Ross, N. Melik-Barkhudarov, K. S. Shankar, A. Wendel, D. Dey, J. A. Bagnell, and M. Hebert, "Learning monocular reactive uav control in cluttered natural environments," in *2013 IEEE International Conference on Robotics and Automation*, May 2013.
- [20] O. Dunkley, J. Engel, J. Sturm, and D. Cremers, "Visual-inertial navigation for a camera-equipped 25g nano-quadrotor," in *IROS2014 Aerial Open Source Robotics Workshop*, 2014.
- [21] A. Briod, J.-C. Zufferey, and D. Floreano, "Optic-flow based control of a 46g quadrotor," in *Workshop on Vision-based Closed-Loop Control and Navigation of Micro Helicopters in GPS-denied Environments, IROS 2013*, no. EPFL-CONF-189879, 2013.
- [22] A. Suleiman, Z. Zhang, L. Carlone, S. Karaman, and V. Sze, "Navion: A fully integrated energy-efficient visual-inertial odometry accelerator for autonomous navigation of nano drones," in *2018 IEEE Symposium on VLSI Circuits*, June 2018, pp. 133–134.
- [23] K. McGuire, G. de Croon, C. de Wagter, B. Remes, K. Tuyls, and H. Kappen, "Local histogram matching for efficient optical flow computation applied to velocity estimation on pocket drones," in *2016 IEEE International Conference on Robotics and Automation (ICRA)*, May 2016.
- [24] G. Hegde, Siddhartha, N. Ramasamy, and N. Kapre, "CaffePresso: An optimized library for Deep Learning on embedded accelerator-based platforms," in *2016 International Conference on Compilers, Architectures, and Synthesis of Embedded Systems (CASES)*, Oct. 2016, pp. 1–10.
- [25] D. Kang, E. Kim, I. Bae, B. Egger, and S. Ha, "C-GOOD: C-code Generation Framework for Optimized On-device Deep Learning," in *Proceedings of the International Conference on Computer-Aided Design*, ser. ICCAD '18. New York, NY, USA: ACM, 2018, pp. 105:1–105:8.
- [26] A. Lokhmotov, N. Chunosov, F. Vella, and G. Fursin, "Multi-objective Autotuning of MobileNets Across the Full Software/Hardware Stack," in *Proceedings of the 1st on Reproducible Quality-Efficient Systems Tournament on Co-Designing Pareto-Efficient Deep Learning*, ser. ReQuEST '18. New York, NY, USA: ACM, 2018.
- [27] L. Lai, N. Suda, and V. Chandra, "CMSIS-NN: Efficient Neural Network Kernels for Arm Cortex-M CPUs," *arXiv:1801.06601 [cs]*, Jan. 2018.
- [28] M. Peemen, A. Setio, B. Mesman, and H. Corporaal, "Memory-centric accelerator design for Convolutional Neural Networks," in *2013 IEEE 31st International Conference on Computer Design (ICCD)*, Oct. 2013, pp. 13–19.
- [29] C. Zhang, P. Li, G. Sun, Y. Guan, B. Xiao, and J. Cong, "Optimizing FPGA-based Accelerator Design for Deep Convolutional Neural Networks," in *Proceedings of the 2015 ACM/SIGDA International Symposium on Field-Programmable Gate Arrays*, ser. FPGA '15. New York, NY, USA: ACM, 2015, pp. 161–170.
- [30] K. He, X. Zhang, S. Ren, and J. Sun, "Deep residual learning for image recognition," in *Proceedings of the IEEE conference on computer vision and pattern recognition*, 2016.
- [31] M. Gautschi, P. D. Schiavone, A. Traber, I. Loi, A. Pullini, D. Rossi, E. Flamand, F. K. Gürkaynak, and L. Benini, "Near-threshold risc-v core with dsp extensions for scalable iot endpoint devices," *IEEE Transactions on Very Large Scale Integration (VLSI) Systems*, vol. 25, no. 10, Oct 2017.
- [32] A. Pullini, D. Rossi, G. Haugou, and L. Benini, "uDMA: An autonomous I/O subsystem for IoT end-nodes," in *2017 27th International Symposium on Power and Timing Modeling, Optimization and Simulation (PATMOS)*, Sep. 2017, pp. 1–8.
- [33] D. E. Bellasi and L. Benini, "Smart energy-efficient clock synthesizer for duty-cycled sensor socs in 65 nm/28nm cmos," *IEEE Transactions on Circuits and Systems I: Regular Papers*, vol. 64, no. 9, pp. 2322–2333, Sept 2017.
- [34] A. Rahimi, I. Loi, M. R. Kakoe, and L. Benini, "A Fully-Synthesizable Single-Cycle Interconnection Network for Shared-L1 Processor Clusters," in *2011 Design, Automation & Test in Europe*. IEEE, Mar. 2011, pp. 1–6.
- [35] F. Conti, D. Palossi, A. Marongiu, D. Rossi, and L. Benini, "Enabling the heterogeneous accelerator model on ultra-low power microcontroller platforms," in *2016 Design, Automation Test in Europe Conference Exhibition (DATE)*, March 2016.
- [36] I. Hubara, M. Courbariaux, D. Soudry, R. El-Yaniv, and Y. Bengio, "Quantized Neural Networks: Training Neural Networks with Low Precision Weights and Activations," *arXiv:1609.07061 [cs]*, Sep. 2016.
- [37] A. S. Razavian, H. Azizpour, J. Sullivan, and S. Carlsson, "CNN features off-the-shelf: An astounding baseline for recognition," in *IEEE Conference on Computer Vision and Pattern Recognition Workshops (CVPRW)*, jun 2014.
- [38] L. Cecconi, S. Smets, L. Benini, and M. Verhelst, "Optimal tiling strategy for memory bandwidth reduction for cnns," in *Advanced Concepts for Intelligent Vision Systems*, J. Blanc-Talon, R. Penne, W. Philips, D. Popescu, and P. Scheunders, Eds. Cham: Springer International Publishing, 2017.
- [39] D. Palossi, J. Singh, M. Magno, and L. Benini, "Target following on nano-scale unmanned aerial vehicles," in *2017 7th IEEE International Workshop on Advances in Sensors and Interfaces (IWASI)*, June 2017, pp. 170–175.
- [40] P. Kumar, S. Garg, A. Singh, S. Batra, N. Kumar, and I. You, "Mvo-based two-dimensional path planning scheme for providing quality of service in uav environment," *IEEE Internet of Things Journal*, 2018.
- [41] C. Yin, Z. Xiao, X. Cao, X. Xi, P. Yang, and D. Wu, "Offline and online search: Uav multiobjective path planning under dynamic urban environment," *IEEE Internet of Things Journal*, vol. 5, no. 2, April 2018.
- [42] D. Palossi, A. Marongiu, and L. Benini, "Ultra low-power visual odometry for nano-scale unmanned aerial vehicles," in *Design, Automation Test in Europe Conference Exhibition (DATE)*, 2017, March 2017.
- [43] D. Falanga, A. Zanchettin, A. Simovic, J. Delmerico, and D. Scaramuzza, "Vision-based autonomous quadrotor landing on a moving platform," in *2017 IEEE International Symposium on Safety, Security and Rescue Robotics (SSRR)*, Oct 2017.
- [44] J. Förster, M. Hamer, and R. D'Andrea, "System identification of the crazyflie 2.0 nano quadcopter," B.S. thesis, 2015.
- [45] R. Mahony, V. Kumar, and P. Corke, "Multirotor aerial vehicles: Modeling, estimation, and control of quadrotor," *IEEE Robotics & Automation Magazine*, vol. 19, no. 3, sep 2012.